Properties of ultrasonic acoustic resonances for exploitation in comb construction by social hornets and honeybees

Jonathan Kadmon*
School of Physics and Astronomy, Raymond and Beverly Sackler Faculty of Exact Sciences, Tel Aviv University, IL-69978 Tel Aviv, Israel

Jacob S. Ishay†
Department of Physiology and Pharmacology, Sackler Faculty of Medicine, Tel Aviv University, Tel Aviv 69978, Israel

David J. Bergman
School of Physics and Astronomy, Raymond and Beverly Sackler Faculty of Exact Sciences, Tel Aviv University, IL-69978 Tel Aviv, Israel and Department of Physics, The Ohio State University, Columbus, Ohio 43210, USA

(Received 9 December 2008; published 9 June 2009)

Physical and mathematical considerations are presented in support of the suggestion that social hornets and bees, which construct brood combs with large arrays of cells in a honeycomb structure, exploit ultrasonic acoustic resonances in those cells in order to achieve the great accuracy of the hexagonal symmetry exhibited by these honeycomb-structured arrays. We present a numerical calculation of those resonances for the case of a perfect-hexagon duct utilizing a Bloch-Floquet-type theorem. We calculate the rate of energy dissipation in those resonances and use that, along with other considerations, to identify the resonance that is best suited for the suggested use by bees and hornets. Previously recorded ultrasonic data on social hornets and honeybees are cited which agree with some of our predictions and thus provide support for the above-mentioned suggestion.

DOI: 10.1103/PhysRevE.79.061909 PACS number(s): 87.10.−e, 51.40.+p, 43.80.+p, 43.20.+g

I. INTRODUCTION

In a previous paper, it was suggested that social hornets and bees might exploit a lateral ultrasonic acoustic resonance in the construction of their brood combs [1]. By adjusting such a resonance in one comb cell to be twofold degenerate, they could ensure that the cell has an accurate perfect-hexagon cross section. Also, by adjusting two adjacent cells to have the same resonance frequency, they could ensure that those cells have cross sections of the same size. Quantitative estimates of the possible resonance frequencies in the case of an oriental hornet comb were obtained by taking the cell cross section to be a circle, instead of the actual perfect-hexagon shape. The expectation was that the resonance used by those hornets has a frequency of about 20 kHz.

In this paper we present some results which provide more evidence in support of the above-mentioned suggestion: we describe results of computations on cells with the correct perfect-hexagon shape and calculate the energy dissipation from those results. From purely mathematical and physical considerations, we identify one lateral resonance which is best suited for the uses that were suggested in Ref. [1]. We present some evidence that the same resonance mode is also used by honeybees in the construction of their brood combs. In that case, the actual resonance frequency will be higher, i.e., in the range of 35–40 kHz. That is because the honeybee comb cells are somewhat smaller than those of the oriental hornet.

In Sec. II we briefly describe the main elements of our numerical computation and present its most important results where the air is modeled as an ideal fluid, the ducts are infinitely long, and the duct walls are perfectly rigid and smooth. In Sec. III we discuss a more realistic model where the air is a real fluid, with viscosity and heat conductivity, and the duct walls are rough, and present some calculations of the energy dissipation. In Sec. IV we discuss the consequences which follow from those results vis-à-vis the exploitation by hornets and bees of ultrasonic resonances in individual comb cells. In Sec. V we summarize our main results and discuss what needs to be done in order to test our predictions.

II. LATERAL ACOUSTIC RESONANCE IN A PERFECT-HEXAGON DUCT FILLED WITH IDEAL FLUID

The lateral acoustic resonances in a cell with a constant perfect-hexagon cross section can be described by writing the following form for the space- and time-dependent pressure oscillations in the cell, the axis of which is taken to be the z-coordinate axis (c is the velocity of sound in air):

$$p_{mn}(\rho,\varphi,t) = e^{im\varphi - ic\alpha_{mn}t}\psi_{mn}(\rho,\varphi), \tag{2.1}$$

where

$$m = 0, \pm 1, \pm 2, 3, \quad n = 1, 2, \ldots .$$

Here we are using cylindrical coordinates (ρ,φ,z) around the cell axis. The appearance of the complex exponential function $e^{im\varphi}$ is a consequence of the hexagonal symmetry in the xy plane: the invariance of the perfect hexagon under rotation by $\pi/3$ rad around the z axis leads to a Bloch-Floquet-type theorem which forces the wave function $\psi_{mn}(\rho,\varphi)$ to be periodic in the azimuthal angle φ with a period of $\pi/3$ rad. We assume that the air in the cell behaves as an ideal fluid

*jona7@post.tau.ac.il
†Deceased.

TABLE I. The lowest eigenvalues $a\alpha_{mn}$ of Eq. (2.2) with Neumann boundary conditions on a perfect hexagon. The degeneracy of eigenvalues with m and $-m$ is exact. Emphasized in boldface is the lowest nonzero (degenerate) eigenvalue; its significance is explained in Sec. IV.

n	$a\alpha_{0n}$	$a\alpha_{\pm 1n}$	$a\alpha_{\pm 2n}$	$a\alpha_{3n}$
1	0	**2.0165**	3.3052	4.1967
2	4.2026	5.7543	5.7944	5.0019
3	7.2707	7.0763	7.4238	8.4015
4	8.3957	8.9869	9.8049	9.184
5	8.4813	9.8496	10.5929	11.0941
6	11.116	11.4358	11.3595	11.8618
7	12.5961	12.8575	12.6416	12.5965
8	13.0647	13.8157	13.9634	13.0466
9	14.5376	14.2964	14.6717	15.1391

and that the cell walls are infinitely rigid and smooth. Then the function $e^{im\varphi}\psi_{mn}(\rho,\varphi)$ is an eigenfunction of the two-dimensional (2D) Helmholtz equation,

$$\left(\frac{\partial^2}{\partial x^2}+\frac{\partial^2}{\partial y^2}+\alpha_{mn}^2\right)e^{im\varphi}\psi_{mn}(\rho,\varphi)=0 \tag{2.2}$$

with Neumann boundary conditions (i.e., vanishing of the normal derivative) on the edges of a perfect hexagon. Each of these eigenstates represents a nonpropagating acoustic mode in the cell, which lies at the bottom of an entire band of propagating modes given by

$$e^{im\varphi+i\gamma_{mn}(\omega)z-i\omega t}\psi_{mn}(\rho,\varphi), \tag{2.3}$$

where

$$\gamma_{mn}^2(\omega)+\alpha_{mn}^2=\frac{\omega^2}{c^2}. \tag{2.4}$$

Equation (2.2) with boundary conditions on a hexagon cannot be simplified by separation of variables. We therefore solved it numerically by discretizing the xy plane, using a triangular grid of points and using the values of $e^{im\varphi}\psi_{mn}(\rho,\varphi)$ at those points in order to compute a finite difference approximation for each of the partial derivatives in that equation and in the boundary condition. This procedure transforms the eigenvalue problem of Eq. (2.2) into a standard eigenvalue problem of a finite Hermitian matrix, whose size depends on the number of grid points. That matrix eigenvalue problem was solved by a standard numerical algorithm on a desktop personal computer. Details of this procedure, as well as some of its surprising mathematical aspects, will be described elsewhere [2].

Some of the main properties of these eigenstates can be seen by considering the low-lying normalized eigenvalues $a\alpha_{mn}$ (a is the edge length of the perfect hexagon) that are listed in Table I. When normalized in this way, the eigenvalues $a\alpha_{mn}$ are pure numbers that are independent of a. We note that the eigenvalues α_{1n} and α_{-1n} are always exactly the same. A similar situation holds for the eigenvalues α_{2n} and α_{-2n}. This twofold degeneracy is a consequence of the perfect-hexagon symmetry. It can also be understood by noting that the eigenfunctions $e^{i\varphi}\psi_{1n}$ and $e^{2i\varphi}\psi_{2n}$ are necessarily complex valued. Therefore their complex conjugates $e^{-i\varphi}\psi_{1n}^*\equiv e^{-i\varphi}\psi_{-1n}$ and $e^{-2i\varphi}\psi_{2n}^*\equiv e^{-2i\varphi}\psi_{-2n}$ are eigenfunctions that differ from the previous two but have the same eigenvalues. By contrast, the eigenfunctions ψ_{0n} and $e^{3i\varphi}\psi_{3n}$ are real valued, and their eigenvalues are not the same (note that although the function ψ_{3n} is complex valued and periodic, the function $e^{3i\varphi}\psi_{3n}$ is real valued and simply changes its sign when $\varphi\rightarrow\varphi+\pi/3$). Both of the two lowest nonzero eigenvalues, $\alpha_{11}\approx 2.0165/a$ and $\alpha_{21}\approx 3.3052/a$, are twofold degenerate and are well separated from each other and from all of the higher eigenvalues. In Sec. IV we will argue that this property of the lowest two eigenvalues makes them of most interest for the application to comb construction. By contrast, each of the higher eigenvalues is fairly close to, sometimes even very close to, another eigenvalue (see, e.g., the pair α_{31} and α_{02} or the pair α_{12} and α_{22}).

Actually, because the twofold-degenerate Bloch-function eigenmodes of Eq. (2.1) are complex-valued functions, they cannot represent any possible physical resonance. A twofold-degenerate resonance with real values of the pressure and the velocity can be obtained as the real or imaginary part of either one of those twofold-degenerate Bloch functions. The resulting real eigenfunctions can be organized so as to be either even or odd under reflection through any one of the six lines of reflection symmetry of the perfect hexagon. In fact, these six lines consist of three pairs of mutually perpendicular lines, where the two operators associated with any single pair of reflection lines commute, while the operators resulting from different pairs of reflection lines do not commute. Therefore the real-valued eigenfunctions can always be organized so as to be the eigenstates of any one of those pairs of operators, but usually not of two pairs simultaneously. Obviously, none of these functions will be a Bloch function, but it will be an eigenfunction of the rotation by an angle π, which is the same as space inversion through the origin, i.e., the transformation $\mathbf{r}\rightarrow-\mathbf{r}$. An example is shown in Fig. 1, where the two degenerate eigenfunctions of each of the two lowest nonzero eigenvalues, namely, $\alpha_{\pm 11}$ and $\alpha_{\pm 21}$, are organized as real-valued functions that are either even or odd under reflection through the midaxis of the exhibited triangle.

It is interesting to compare the perfect-hexagon eigenvalues of Table I with the eigenvalues of Helmholtz equation with Neumann boundary conditions on a circle of radius b. These eigenvalues, denoted by β_{mn}, are obtained from zeros of the first derivative of the Bessel function J_m [1],

$$J_m'(\beta_{mn}b)=0. \tag{2.5}$$

Some of those eigenvalues are shown in Table II. They exhibit similar properties to those described above for α_{mn}: both of the two lowest nonzero eigenvalues, $\beta_{11}\approx 1.841/b$ and $\beta_{21}\approx 3.054/b$, are twofold degenerate and are well separated from each other and from all the higher eigenvalues. Again, each of the higher eigenvalues is close to another eigenvalue. This approximate degeneracy becomes more and more pronounced with increasing n due to the mathematical properties of the Bessel functions for large arguments, i.e.,

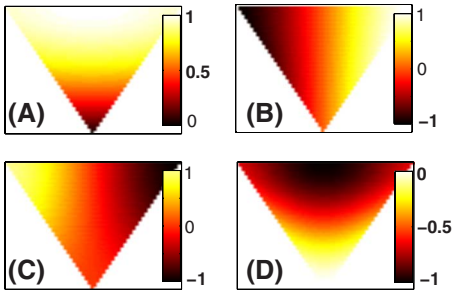

FIG. 1. (Color online) Using an appropriate linear combination of the Bloch-type eigenfunctions of the $\pi/3$ rotation operator, one can construct solutions of the Helmholtz equation that are even or odd under reflection through the midaxis of the triangle which constitutes 1/6 of the perfect-hexagon cross section. Panels (A) and (B) are the even and odd functions corresponding to the eigenvalue α_{11} (or α_{-11}), while panels (C) and (D) are the odd and even functions corresponding to the eigenvalue α_{21} (or α_{-21}). For clarity, each of those functions is normalized, so that its values span the entire interval $[0,1]$, $[-1,0]$, or $[-1,1]$. Note that the extension of these eigenfunctions to the other five triangular sections of the perfect hexagon is nonperiodic (see, e.g., Fig. 2).

the fact that $J_m(x) \sim x^{-1/2} \cos(x - m\frac{\pi}{2} - \frac{\pi}{4})$. Also worth mentioning is the fact, which was expected previously, that each of the lowest eigenvalues for the perfect hexagon lies in between that of the circumscribing circle (with radius $b=a$) and that of the circumscribed circle (with radius $b=\sqrt{3}a/2$) [1].

III. EFFECTS OF DISSIPATION

In real air, the acoustic resonance decays in time due to a variety of processes that were hitherto neglected. One of those is the energy dissipation due to nonideal fluid flow near the boundary: for a nonideal fluid, both the normal and the tangential velocities at the surface of the cell walls must vanish. As a result, the velocity parallel to the wall increases from zero at the wall up to its ideal fluid value over a viscous penetration depth [5]. The rate of energy loss in this so-called boundary layer is directly related to the tangential velocity found at the boundary for an ideal fluid. The ideal fluid velocity of each lateral mode at the wall can be obtained from the tangential gradient $\partial p_{mn}/\partial x$ of the local pressure [see Eq. (2.1)] and using Euler's equation,

$$\frac{dv_{mn}(\mathbf{r},t)}{dt} = -i\omega_{mn} v_{mn}(\mathbf{r},t) = -\frac{1}{\rho}\frac{\partial p_{mn}(\mathbf{r},t)}{\partial x}, \tag{3.1}$$

where x is the fluid coordinate parallel to the wall, ρ is the fluid mass density, $v_{mn}(\mathbf{r},t)$ is the tangential velocity of the mn eigenstate at the wall, and $\omega_{mn} \equiv c\alpha_{mn}$ is the angular frequency of that eigenstate.

In the solution for a circular boundary, the tangential gradient is just the projection of ∇p_{mn} along the azimuthal unit vector $\mathbf{e}_\varphi$, and the tangential velocity can be calculated in a simple closed form. Examining the two lowest normalized acoustic modes, which are of most interest to us, p_{11} and p_{21}, it is easy to show that the tangential velocity of the latter is almost twice as large as that of the former. This results from the velocity amplitude being proportional to the m index and to the peak value of $J_m(\beta_{mn}r)$.

In the case of a perfect-hexagon boundary condition, we need to be somewhat more careful, even before we numerically compute the tangential pressure gradient $\partial p_{mn}/\partial x$ along the straight wall segments: as explained in the previous section, the physical resonance pressure p_{phys} must be some real-valued linear combination of $\text{Re}(p_{mn})$ and $\text{Im}(p_{mn})$, namely,

$$p_{\text{phys}} = A\ \text{Re}(p_{mn}) + B\ \text{Im}(p_{mn}). \tag{3.2}$$

From this it follows that the physical value of the tangential velocity v_{phys} will be a similar combination, namely,

$$v_{\text{phys}} = \frac{1}{\rho\omega_{mn}}\left[-A\ \text{Im}\left(\frac{\partial p_{mn}}{\partial x}\right) + B\ \text{Re}\left(\frac{\partial p_{mn}}{\partial x}\right)\right]. \tag{3.3}$$

By choosing a real time dependence of the form $\cos(\omega_{mn}t + \delta)$, the eigenfunction becomes a real time-dependent standing wave. In Fig. 2 we plot the amplitude of the tangential velocity vs position along the circumference of the hexagon for the four standing waves whose wave functions were plotted in Fig. 1: the even and the odd (with respect to reflection through $\varphi=\pi/6$) standing waves of the α_{11} and α_{21} eigenvalues [4]. These standing waves are all normalized to 1 in L_2, i.e., their squared values integrate to 1 over the area of the hexagon. It can be seen that the tangential velocity at the boundary is lower for the eigenstates with the lower eigenvalue α_{11}.

The value of the velocity at the boundary is very important when attempting to estimate the width of the actual peak in the frequency spectrum, namely, the sharpness of the reso-

TABLE II. The lowest eigenvalues $b\beta_{mn}$ of Eq. (2.2) with Neumann boundary conditions on a circle of radius b (see Refs. [1,3] for details). Eigenvalues with $\pm m$ are degenerate. The relevance of the lowest nonzero (degenerate) eigenvalue $\beta_{\pm 1,1}$, which is emphasized in boldface, is discussed in Sec. IV.

n	$b\beta_{0n}$	$b\beta_{\pm 1n}$	$b\beta_{\pm 2n}$	$b\beta_{\pm 3n}$	$b\beta_{\pm 4n}$	$b\beta_{\pm 5n}$
1	0	**1.841**	3.054	4.201	5.317	6.416
2	3.832	5.331	6.706	8.015	9.282	10.520
3	7.016	8.536	9.969	11.346	12.682	13.987
4	10.173	11.706	13.170	14.586	15.964	17.313
5	13.324	14.864	16.347	17.789	19.196	20.575

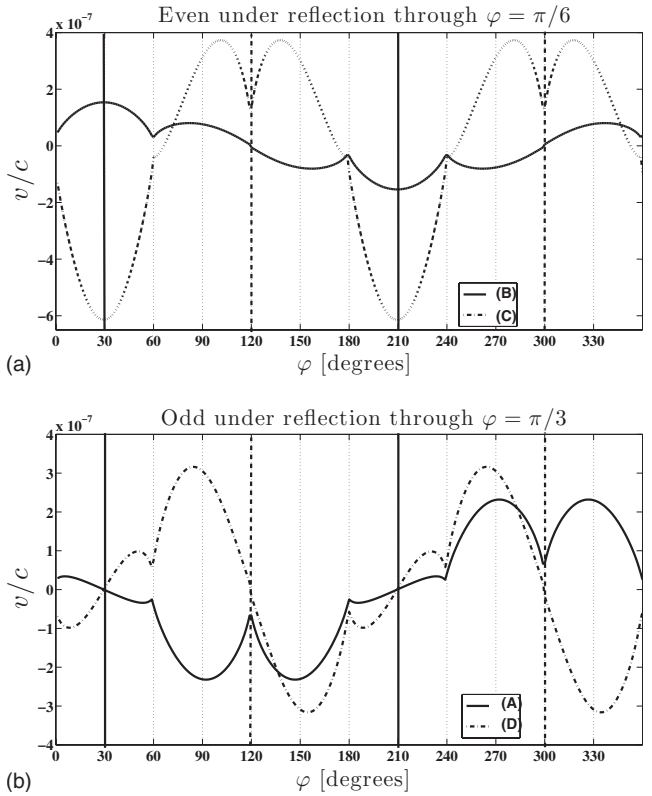

FIG. 2. The ideal fluid tangential velocity amplitude of air, at the walls of a perfect-hexagon cell, in the two lowest lateral normalized eigenstates, v_{11} and v_{21}, plotted vs the azimuthal coordinate φ along the wall, as obtained numerically from Eq. (3.3). The eigenfunctions are constructed so as to be real valued and are either even or odd under reflection through the midaxis $\varphi=\pi/6$ of the original triangle. In agreement with the notation of Fig. 1, (A) and (B) denote the odd and even velocity functions corresponding to the eigenvalue α_{11} (or α_{-11}), while (C) and (D) denote the even and odd velocity functions corresponding to the eigenvalue α_{21} (or α_{-21}) [4]. The solid vertical lines mark the position of the above-mentioned reflection axis. The dashed vertical lines mark the position of the other reflection axis in the commuting pair of reflection symmetries, which is perpendicular to the previous one.

nance. The width of the peak in frequency space is directly related to the rate of energy loss due to dissipation. The typical lifetime of a free oscillation can be expressed by the ratio [5]

$$\tau = \frac{\bar{E}}{\overline{|\dot{E}_{kin}|}}, \tag{3.4}$$

where $\overline{\dot{E}_{kin}}$ is the time averaged rate of (kinetic) energy loss per unit volume due to dissipation and $\bar{E}$ is the time averaged energy per unit volume in the system given by the expression

$$\bar{E} = \frac{1}{2}\rho \int_V v_0^2(\mathbf{r}) d^3r, \tag{3.5}$$

in which $v_0(\mathbf{r})$ is the local amplitude of the velocity field in the ideal fluid.

In order to calculate the rate of energy dissipation in the boundary layer, we treat the system as a nonideal fluid and impose the correct boundary conditions under which both normal and tangential velocities vanish at the wall. The tangential velocity then changes from zero at the boundary to its ideal fluid value over a thin viscous penetration depth given by

$$\xi(\omega) \equiv \sqrt{\frac{2\eta}{\omega\rho}}, \tag{3.6}$$

where η is the fluid shear viscosity. The rate of energy loss in that boundary layer is given by the expression [5]

$$\overline{|\dot{E}_{kin}|} = \frac{1}{2}\sqrt{\frac{1}{2}\omega\eta\rho}\int_{\partial V} v_0^2(\mathbf{r}) d^2r, \tag{3.7}$$

in which the surface integral is taken over the fluid boundary ∂V.

Using our numerical solution for the eigenfunctions, we were able to calculate the full width at half maximum $\delta\omega$ of the resonance peak as follows:

$$\delta\omega \equiv \tau^{-1} = \sqrt{\frac{\omega\eta}{2\rho}}\frac{\int_{\partial V} v_0^2(\mathbf{r}) d^2r}{\int_V v_0^2(\mathbf{r}) d^3r} \equiv \sqrt{\frac{\omega\eta}{2\rho}}\frac{A_{mn}}{a} \propto \frac{1}{a^{3/2}}, \tag{3.8}$$

where A_{mn} is a dimensionless quantity independent of a. By numerical integration of our results for the velocity field, we find $A_{11}=1.0123$ for both the even and odd eigenfunctions with the eigenvalue α_{11} [6]. This leads to the following estimate for the relative width of that resonance due to viscous dissipation in the boundary layer:

$$\frac{\delta\omega_{11}}{\omega_{11}} = \sqrt{\frac{\frac{1}{2}\eta}{\alpha_{11}ac}}\frac{1}{\sqrt{a}}A_{11} = 3.16\times 10^{-6}\frac{1}{\sqrt{a}}, \tag{3.9}$$

where we used $\omega=\omega_{mn}=c\alpha_{mn}$, as well as the shear viscosity of air at 300 K (see below). The final result of Eq. (3.9) assumes that the cell edge a is given in millimeters. Evidently, the relative peak width is proportional to $1/\sqrt{a}$, while the absolute peak width is proportional to $a^{-3/2}$. Moreover, by using Eqs. (3.6) and (3.8) we find that

$$\frac{\xi(\omega_{mn})}{a} = \frac{4}{A_{mn}}\frac{\delta\omega_{mn}}{\omega_{mn}} \tag{3.10}$$

Equation (3.10) allows us to verify our assumption of a thin viscous penetration depth $\xi(\omega_{mn}) \ll a$ for the lowest eigenstates.

In fact, Eq. (3.8) only gives a lower bound for the width of the resonance since there are other sources of dissipation which can further attenuate the system response. Some of those are the dissipation of acoustic oscillations in bulk air, the penetration of those oscillations into the porous cell walls, and interaction of lateral resonance modes with other propagating acoustic modes via the nonperfect smoothness and nonperfect rigidity of the cell walls. We now briefly

discuss these effects in order to gauge their importance.

The broadening of the resonance peak, due to viscosity and thermal conductivity of the bulk fluid, is given by [5]

$$\delta\omega_{bulk} = \frac{\omega^2}{\rho c^2}\left[\frac{4}{3}\eta + \zeta + \kappa\left(\frac{1}{C_V} - \frac{1}{C_P}\right)\right], \qquad (3.11)$$

where η and ζ are the shear viscosity and bulk viscosity, respectively; κ is the thermal conductivity; and C_V and C_P are the heat capacities at constant volume and constant pressure. In order to evaluate Eq. (3.11) we use properties of dry air at 300 K: $C_P = 1.0049$ kJ/kg K, $C_V = 0.7178$ kJ/kg K, $\kappa = 2.624 \times 10^{-5}$ kW/m K, $\eta = 1.846 \times 10^{-5}$ kg/m s, $\rho = 1.177$ kg/m^3, and $c = 330$ m/s. For the bulk viscosity we use the results of Greenspan who showed that $\zeta = 0.60\eta$ [7]. The relative peak broadening for the acoustic mode p_{11}, due to dissipation of sound in bulk air, is thus found to be

$$\left.\frac{\delta\omega_{11}}{\omega_{11}}\right|_{bulk} = \frac{\alpha_{11}}{\rho c}\left[1.93\eta + \kappa\left(\frac{1}{C_V} - \frac{1}{C_P}\right)\right] = 1.6 \times 10^{-8}\frac{1}{a}, \qquad (3.12)$$

where a is again measured in mm. We note that the result is proportional to $1/a$ since $\alpha_{mn}a$ is independent of a. Comparing Eqs. (3.9) and (3.12), we find that the broadening of the peak arising from the viscous boundary layer is greater than the broadening due to viscosity and thermal conductivity in bulk air for systems of linear size $a > 2.5 \times 10^{-2}$ mm. In the construction of a brood comb, as discussed in Sec. IV, the size a is several millimeters and is thus well within that limit. Therefore, bulk acoustic dissipation contributes a negligible amount to the peak broadening, as compared to shear motion in the viscous boundary layer.

The walls of the cell in a brood comb of hornets are forged from a cement which the hornets make by mixing cellulose fibers and gravel with their saliva [8,9]. Upon drying, this solidifies into a soft solid with small air-filled pores. The motion of that air is strongly damped by viscosity and friction with the pore walls. This provides a mechanism of energy dissipation which cannot be addressed seriously without knowing more details about the pore structure and the penetration of the acoustic oscillations into the walls. Thus, the result for resonance width given by Eq. (3.9) is actually only a lower bound.

Each of the eigenvalues listed in Tables I and II represents the nonpropagating mode which lies at the bottom of a band of propagating modes (except for the band starting at zero, since there is no mode at $\omega = 0$). In other words, each lateral mode is degenerate with propagating modes in bands that start at a lower frequency. Due to the roughness and the nonperfect rigidity of the walls, different modes can usually interact and transfer energy to each other. Consequently, energy is carried outward by the propagating modes and this weakens the resonant response of the lateral modes. This applies to all the lateral resonances except the lowest one. That mode only overlaps with the lowest band p_{01} of propagating modes, which are longitudinal waves with frequencies that start from $\omega = 0$. However, because these propagating modes involve no lateral motion, they therefore do not interact with lateral modes. Thus, p_{11} is the only lateral mode that has no interaction with any propagating modes. We note that the hidden assumption of an infinite duct is used for convenience, but is not essential, since the lateral modes are nonpropagating modes. Any interaction of a lateral mode with standing waves of a semiopen duct would also result in some loss of energy to the outside.

IV. CONSEQUENCES FOR COMB CONSTRUCTION

In Sec. II we showed that the eigenvalues of some of the nonpropagating acoustic modes of a perfect-hexagon-shaped cell are twofold degenerate, as in the case of a circle. This property can be utilized in order to evaluate the accuracy of symmetry of the cross section along the main axis of a duct in the following manner: by exciting a band of frequencies around the eigenfrequency of a certain twofold-degenerate mode and listening to the acoustic response, a perfectly symmetric cross section can be distinguished from a slightly deformed one. While the first exhibits a single harmonic response, the latter results in the appearance of beats due to the interference of the two slightly different response frequencies. To be more specific, the C_{6v} symmetry of the perfect hexagon has two 2D irreducible representations, while any deformed shape has only one-dimensional (1D) irreducible representations [10]. Moreover, the only cell shapes that have such 2D irreducible representations are the n-sided perfect polygons, namely, the shapes characterized by the C_{nv} symmetry groups with $n > 2$. Any shape with lower symmetry, e.g., rectangles or nonperfect hexagons, has only 1D irreducible representations. By a process of trial and error, the shape of the cell can be fine tuned to exact perfect-hexagon shape, much like how a piano tuner tunes a piano string by listening to it beating against a vibrating tuning fork. We note that although all the cyclic symmetry groups C_{nv} with $n > 2$ have 2D representations, only the limited subset of the n-sided polygons with $n = 3$, 4, or 6 can be used for a regular tessellation of the plane. Of these three shapes, the one that is best suited for efficiently accommodating the body of a hornet or bee is the $n = 6$ perfect-hexagon shape.

The resonance frequencies of the cells can also be used to test for size difference of two adjacent cells: by exciting the same mode in both cells and listening to the low-frequency beats, the same process of trial and error can be applied until the two cells have congruent shape and size [1]. For this procedure to work, some requirements need to be satisfied regarding the resonance frequencies and their corresponding widths. These requirements limit the eigenfrequencies which are suitable. First, we note that the interval between two adjacent eigenfrequencies $\Delta\omega$ must be significantly larger than the resonance width $\delta\omega$ due to dissipation. In Table III the intervals between the first few pairs of adjacent eigenfrequencies are shown using the values presented in Table I. Also shown there are the widths of the peaks in the frequency spectrum, calculated using Eq. (3.8). Standard conditions of dry air at 300 K and a hexagon edge length of 5 mm were used for the calculation of all the frequencies. Noting that the intervals between adjacent eigenfrequencies diminish as the frequency increases, as discussed in Sec. II, we conclude that the only two eigenfrequencies whose distance

TABLE III. Intervals between the first few pairs of adjacent eigenfrequencies, calculated from the values given in Table I, and the peak width of the first few eigenfrequencies, calculated using Eq. (3.8). Standard material parameters of dry air at 300 K (see Sec. III for details) were used and the hexagon edge length was taken to be 5 mm, corresponding to a distance between opposite cell walls of about 9 mm.

Interval $\Delta\omega$ (s^{-1})	Peak width $\delta\omega$ (s^{-1})
$\omega_{21}-\omega_{11}=8.5\times10^4$	$\delta\omega_{11}=239$
$\omega_{31}-\omega_{21}=5.8\times10^4$	$\delta\omega_{21}=551$
$\omega_{02}-\omega_{31}=389$	$\delta\omega_{31}=859$
	$\delta\omega_{02}=579$

from each other and from all the other eigenfrequencies is sufficiently large compared to the relevant peak widths are the lowest two, i.e., ω_{11} and ω_{21}.

Another requirement has to do with the leakage of energy outward via propagating waves. The lateral mode should have minimal interaction with propagating modes. We note however that some leakage might in fact be necessary in order for the oscillations to be detectable. In a real physical system some energy will always exit from the duct. Nevertheless, we believe that the best lateral mode should have minimal interaction with propagating modes. In Sec. III we showed that the lateral mode p_{11} is the only one which has no interaction with other propagating modes and thus is the most suitable one.

Taking into consideration also the results presented in Fig. 2, from which it follows that p_{11} suffers less dissipation due to friction with the wall than p_{21}, we conclude that the lateral mode p_{11} is the most appropriate mode for monitoring the construction of a perfect-hexagon comb cell. The expectation that it is probably easier for insects to produce an acoustic signal at that frequency than at the higher ultrasonic frequency of the mode p_{21} only reinforces that conclusion.

From the absolute width $\delta\omega$ of a resonance, we can deduce the lifetime $\tau\approx 1/\delta\omega$ of such a freely oscillating state. Even in the best case, i.e., the p_{11} resonance, the number in Table III leads to $\tau\approx 5$ ms. That is probably much too short to allow for listening to time-dependent beats as a piano tuner would. Therefore we feel it is more likely that the hornets or bees actually listen to the pitch or frequency of those beats. From the measurements reported in Ref. [11], it is evident that social hornets use audio frequencies around 200 Hz in order to communicate information. Therefore they must hear well at those frequencies and could well be able to judge whether a change in cell construction has increased or decreased a beat frequency by more than the frequency width of the p_{11} peak $\delta\nu_{11}=\delta\omega_{11}/(2\pi)\approx 40$ Hz. The hornets could cope with the short lifetime of these beats (about 5 ms as shown above) by emitting a long train of ultrasonic pulses. Alternatively, they could emit a continuous monochromatic signal, slowly changing its pitch and listening to the change in response of the driven system when the driving frequency happens to coincide, up to $\delta\nu_{11}$, with the resonance frequency of one of the adjacent cells.

In measurements of the sound spectrum near a brood comb of oriental hornets (*Vespa Orientalis*), a small but distinct rise in the background noise was found to occur around 20 kHz [1,11]. Using the results of Sec. II and taking the cell width, i.e., the distance between opposing edges of the cell, to be 10 mm [1], the expected frequency of the p_{11} mode is $\nu_{11}=c\alpha_{11}/2\pi=2.0165(c/2\pi a)=19.6$ kHz. The increase in the background sound intensity, which is documented in Ref. [11], can be attributed to the acoustic response of the honeycomb structure. This observation confirms the existence of a significant acoustic response of the oriental hornet honeycomb structure at the eigenfrequency of the p_{11} mode.

The ability of insects to produce sound in the ultrasonic frequency range is not self-evident and should not be taken for granted. Therefore, it is encouraging that ultrasonic sound production capability of honeybees was detected by Spangler [12]. In that study, which was conducted outside but nearby to a beehive, the ultrasonic sound waves produced by honeybees (*Apis Mellifera L.*) during four types of activities were recorded and their spectrum was analyzed. Spangler notes that the sound energy in all the recordings reached its greatest intensity between 30 and 40 kHz. Using the cell width of a honeycomb constructed by honeybees, namely, 5–6 mm [13], the frequency of the p_{11} mode comes out as $\nu_{11}=35-40$ kHz, in good agreement with Spangler's observation. Noting that the next eigenstate, i.e., p_{21}, would have a frequency $\nu_{11}=55-60$ kHz, we see that the honeybees do not produce such high frequencies, in contrast with their proven ability to produce ultrasound in a narrow band around the p_{11} frequency.

V. DISCUSSION, CONCLUSIONS, AND SUGGESTIONS FOR FURTHER STUDY

We presented and discussed some numerical solutions for eigenstates of the acoustic equation in an ideal fluid inside a perfect-hexagon duct. The results were compared with the closed-form eigenstates of a circular duct which have similar properties. We discussed the various dissipative mechanisms in real air in order to find a lower bound for the finite width of the lateral resonances. We described how the mathematical and physical properties of the solutions can be utilized by hornets and bees in order to construct a brood comb with identical perfect-hexagon-shaped cells and showed, from purely mathematical and physical considerations, that the lowest-lying lateral resonance mode, denoted by p_{11}, is best suited for that application.

The work done by Ishay [11] provides evidence that the oriental hornet combs in fact have a significant acoustic response at a frequency that agrees with our predictions. Nevertheless, more acoustic data are required to further verify the results shown in Sec. II: measurements of a broader acoustic spectrum should be performed for a single hexagonal cell. Such measurements, if performed with appropriate equipment, might show more of the resonances that were calculated numerically in Sec. II. Also, the real peak broadening should be measured since, as mentioned in Sec. II, only a lower bound for this quantity could be calculated.

The first recorded data of honeybees producing ultrasound in the appropriate frequency range were presented by Spangler [12]. In that paper Spangler describes the mechanism which allows the honeybees to produce such frequencies. He also suggested that this ability is used as a means to deter attacks by wax moths that prey on honeybees. The theory presented here provides an alternative explanation for this aptitude. The fact that there is no observed ability of hornets or bees to detect the ultrasonic sounds does not rebut our conjecture since, as explained in Sec. IV, the frequency of the beats themselves is well within their recorded hearing ability.

As a further test of our theory, we would like to suggest that a continuous ultrasonic noise be applied while cell construction is under way. We expect that the construction activity will be disrupted or undermined by such noise if it is loud enough to drown out the ultrasonic signals which are presumably emitted by the hornets or bees engaged in cell construction. Such tests are currently in progress. Another important measurement which needs to be made is to determine the acoustic spectrum inside a brood comb and near a comb cell while its construction is under way. We would like to encourage other researchers to perform such measurements.

[1] D. J. Bergman and J. Ishay, Bull. Math. Biol. **69**, 1777 (2007).
[2] J. Kadmon and D. J. Bergman (unpublished).
[3] A. D. Pierce, *Acoustics* (Acoustical Society of America, New York, 1991), 2nd printing.
[4] Note that the even or odd parity of $p_{mn}(\mathbf{r})$ is *opposite* to that of $v_{mn}(\mathbf{r})$.
[5] L. D. Landau and E. M. Lifshitz, *Fluid Mechanics*, 2nd ed. (Pergamon Press, New York, 1987).
[6] The fact that both the even and the odd eigenfunctions of any eigenvalue yield the same value for A_{mn} is a theorem [2].
[7] M. Greenspan, J. Acoust. Soc. Am. **31**, 155 (1959).
[8] J. S. Ishay and E. Ganor, J. Morphol. **203**, 11 (1990).
[9] J. P. Spradbery, *Wasps* (Sidgwick & Jackson, London, 1973).
[10] L. D. Landau and E. M. Lifshitz, *Quantum Mechanics*, 3rd ed. (Pergamon Press, New York, 1977).
[11] J. Ishay, J. Insect Physiol. **21**, 1737 (1975).
[12] H. H. Spangler, J. Apic. Res. **25**, 213 (1986).
[13] K. von Frisch, *Animal Architecture* (Hutchinson, London, 1975), translated (from German) by L. Gombrich.